

CT reconstruction from parallel and fan-beam projections by 2D discrete Radon transform

Amir Averbuch¹ Ilya Sedelnikov¹ Y. Shkolnisky²

¹School of Computer Science, Tel Aviv University, Tel Aviv 69978

²Program of Applied Mathematics, Department of Mathematics
Yale University, New Haven, CT, USA

September 3, 2006

Abstract

We propose two algorithms for the reconstruction of a 2D object from its continuous projections. The first algorithm operates on parallel projection data, while the second uses the more practical model of fan-beam projections. Both algorithms are based on the discrete Radon transform, which extends the continuous Radon transform to discrete data. The discrete Radon transform and its inverse can be computed in a complexity comparable with the 2D FFT, and are shown to accurately model the continuum as the number of samples increases. Numerical results demonstrate high quality reconstructions for both parallel and fan-beam acquisition geometries.

1 Introduction

The Radon transform is an integral transform whose inverse is used to reconstruct images from medical CT scans. In the 2D case, the Radon transform of a function $f(x, y)$, denoted by

$\Re f(\theta, s)$, is defined as the line integral of f along a line L inclined at an angle θ and at distance s from the origin. Formally,

$$\begin{aligned}\Re f(\theta, s) &= \int_L f(x, y) du \\ &= \int_{-\infty}^{\infty} \int_{-\infty}^{\infty} f(x, y) \delta(x \cos \theta + y \sin \theta - s) dx dy,\end{aligned}\tag{1}$$

where $\delta(x)$ is Dirac's delta function [3]

In CT imaging, $f(x, y)$ is the distribution of the x -ray attenuation coefficient within the object. The goal of CT imaging is to reconstruct $f(x, y)$ from the projections of the object. Each projection is a collection of line integrals as in Eq. (1). Parallel projection and fan-beam projection are two common acquisition geometries. Parallel projection is given by $\Re f(\theta, s)$ with fixed θ and varying s . Fan-beam projection is formed by line integrals along rays that emanate from a single point source.

Due to physical constraints on the size and number of detectors, in practice each projection is comprised of a finite number of line integrals. For parallel projections, this means that $s \in \{s_1, \dots, s_m\}$ for some finite m . Only finite number of projections can be collected, that is $\theta \in \{\theta_1, \dots, \theta_n\}$ for some integer n .

When a single source of radiation is used, fan-beam projections are more efficient, since all measurements in one fan are acquired simultaneously. For this reason, commercial CT scanners use fan-beam projections.

The structure of the paper is as follows. In Section 2 we review related work, namely, fast inversion algorithm of the Radon transform. Section 3 shortly describes the discrete Radon transform [5] together with the results and properties that are relevant to the proposed algorithms. Section 4 demonstrates reconstruction from samples of the continuous Radon transform, which is the basis for reconstruction from fan-beam projections. Finally, in Section 5 we describe reconstruction from fan-beam projections, including the acquisition geometry and the “re-sorting” algorithm.

2 Related works

Tomographic reconstruction underlies nearly all diagnostic imaging modalities, including x-ray computed tomography (CT), positron emission tomography, single photon emission tomography, and certain acquisition methods for magnetic resonance imaging. It is also widely used for nondestructive evaluation in manufacturing, and more recently for airport baggage security. The reconstruction problem in tomography is recovery (inversion) from samples of either the x-ray transform (set of the line-integral projections) or the Radon transform (set of integrals on planes) of an unknown object density distribution. Speedups of these computations are critical for next-generation real-time imaging systems.

Several fast reconstruction algorithms have been proposed. Bresler et. al. [7, 9] uses fast hierarchical algorithms for tomographic reconstruction where filtered backprojection (FBP) is the reconstruction method. In this technique, the FBP is the computational bottleneck with computational requirements of $O(n^3)$ for an $n \times n$ pixel image in two dimensions, and at least $O(n^4)$ for an $n \times n \times n$ voxel image in three dimensions. In [7, 9], they present a family of fast hierarchical tomographic backprojection algorithms, which reduce the complexity to $O(n^2 \log n)$ for the 2D case. The algorithm employs a divide-and-conquer strategy in the image domain, and relies on properties of the harmonic decomposition of the Radon transform. For image sizes typical in medical applications or airport baggage security, this results in speedups by more than an order of magnitude. It is a new fast reconstruction algorithm for parallel beam tomography. This algorithm is an accelerated version of the standard filtered backprojection (FBP) reconstruction. These algorithms provide orders of magnitude speedup in reconstruction time with little or no added distortion. The proposed algorithms are parallelizable, simple, and from their experiments they outperform Fourier Reconstruction Algorithms as well as the MI method in terms of reconstruction distortion and CPU time.

Other fast reconstruction algorithms that exhibit $O(n^2 \log n)$ runtime have been proposed. They include what is known collectively as Fourier reconstruction algorithms (FRA), and mul-

tilelevel inversion (MI) algorithm. FRA are based on Fourier Slice Theorem [2], which states that the Fourier transform of a projection at angle θ is a radial slice through the 2D Fourier transform of the object at direction θ . Before the appearance of our algorithms [4, 5], on which the new algorithms in this paper are based, Fourier reconstruction algorithms have been formed by the following sequence of steps:

1. FFT is applied on the padded projections;
2. A 2D Cartesian FFT grid is interpolated from the polar grid;
3. The image is recovered by a 2D Inverse FFT.

The difficulty lies in step 2. The interpolation step introduces distortions into the reconstruction, since the Fourier transform is sensitive to these interpolations. The method of gridding in [10] for the reconstruction was used in [7] for comparison with their performance.

The paper [7] claims and proves that it outperforms Fourier reconstruction algorithms [10] and the multilevel inversion algorithm by Brandt et al. [6], both of which also have $O(n^2 \log n)$ cost. It also suggests that the proposed hierarchical scheme has a superior cost versus distortion performance. Both methods are described in details in [7].

The proposed algorithms in this paper are simpler in comparison to [7]. In fact, they can be implemented using only 1D FFTs. The transforms underlying these algorithms are proven in [4, 5] to be algebraically accurate, preserve the geometric properties of the continuous transforms, invertible, and rapidly computable. In addition, it is shown in [5] that the discrete Radon transform converges to the continuous Radon transform, as the discretization step goes to zero. This property is of major theoretical and computational importance since it shows that the discrete transform is indeed an approximation of the continuous transform, and thus can be used to replace the continuous transform in digital implementations.

3 2D discrete Radon transform

A 2D discrete Radon transform is defined in [5] as an analogue of the continuous Radon transform for discrete images. The definition is based on summation along lines of absolute slope less than 1. Lines of the form $y = ax + b$ where $|a| \leq 1$ are called “basically horizontal”, and lines of the form $x = ay + b$ with $|a| \leq 1$ are called “basically vertical”. Values at non-grid locations are defined using shear transforms (see [4, 5]). Following [5], we denote the 2D discrete Radon transform of a discrete image I along the line $y = sx + t$ by $Radon(\{y = sx + t\}, I)$. The discrete 2D definition of the Radon transform is shown in [5] to be geometrically faithful as the lines used for summation exhibit no wraparound effects. We also show that it satisfies the Fourier slice theorem, which states that the 1D Fourier transform of the discrete Radon transform is equal to the samples of the pseudo-polar Fourier transform of the underlying image that lie along a ray.

There exists a special set of parallel projections for which the transform is rapidly computable and invertible. For a discrete image $I(u, v)$, $u, v \in [-n/2 : n/2 - 1]$, this set consists of $n + 1$ basically horizontal and $n + 1$ basically vertical projections, given by the sets

$$S_H(t, l) = \left\{ y = \frac{2l}{n}x + t \right\} \quad \text{and} \quad S_V(t, l) = \left\{ x = \frac{2l}{n}y + t \right\},$$

where $l \in [-\frac{n}{2} : \frac{n}{2}]$ and $t \in [-n : n]$.

For a fixed $l \in [-\frac{n}{2} : \frac{n}{2}]$, the l -th basically horizontal projection is composed of summations along lines from the set $S_H(\cdot, l) = \{y = \frac{2l}{n}x + t \mid t \in [-n : n]\}$. The l -th basically vertical projection is composed of summations along lines from the set $S_V(\cdot, l) = \{x = \frac{2l}{n}y + t \mid t \in [-n : n]\}$. We denote the results from these discrete summations by $P_H(t, l) = Radon(S_H(t, l), I)$ and $P_V(t, l) = Radon(S_V(t, l), I)$, $l \in [-\frac{n}{2} : \frac{n}{2}]$ and $t \in [-n : n]$.

We prove in [5] that if the image $I(u, v)$ consists of samples of the function $f(x, y)$ on a Cartesian grid, then the 2D discrete Radon transform of $I(u, v)$ approximates the continuous parallel projections of $f(x, y)$. Rephrasing the convergence theorem in [5], we have the following result:

Theorem 3.1. Assume $f(x, y) \in Lip_\alpha(\mathbb{R})$ that equals to zero outside the square $(-1 + \varepsilon, 1 + \varepsilon) \times (-1 + \varepsilon, 1 - \varepsilon)$ for some $\varepsilon > 0$. Define $I_n(u, v) = f(u \frac{2}{n}, v \frac{2}{n})$, $n \in \mathbb{N}$. Then, for $n \rightarrow \infty$

$$\left| \text{Radon}(\{y = \frac{2l}{n}x + t\}, I_n) \cdot \frac{2}{n} - \int_{-\infty}^{\infty} f(x, \frac{2l}{n}x + \frac{2t}{n}) dx \right| \longrightarrow 0$$

and

$$\left| \text{Radon}(\{x = \frac{2l}{n}y + t\}, I_n) \cdot \frac{2}{n} - \int_{-\infty}^{\infty} f(\frac{2l}{n}y + \frac{2t}{n}, y) dy \right| \longrightarrow 0$$

uniformly for $l \in [-\frac{n}{2} : \frac{n}{2}]$ and $t \in [-n : n]$.

In particular, this theorem establishes the correspondence between the lines in the “discrete” domain and the lines in the “continuous” domain. By analogy with S_H and S_V in the discrete domain, we define two sets of lines in the continuous domain

$$\tilde{S}_H(t, l) = \left\{ y = \frac{2l}{n}x + \frac{2t}{n} \right\} \quad \text{and} \quad \tilde{S}_V(t, l) = \left\{ x = \frac{2l}{n}y + \frac{2t}{n} \right\},$$

where $l \in [-\frac{n}{2} : \frac{n}{2}]$ and $t \in [-n : n]$. We denote line integrals along these lines by $\tilde{P}_H(t, l) = \int_{-\infty}^{\infty} f(x, \frac{2l}{n}x + \frac{2t}{n}) dx$ and $\tilde{P}_V(t, l) = \int_{-\infty}^{\infty} f(\frac{2l}{n}y + \frac{2t}{n}, y) dy$. By Theorem 3.1, $P_H(t, l) \cdot \frac{2}{n}$ converges to $\tilde{P}_H(t, l)$ and $P_V(t, l) \cdot \frac{2}{n}$ converges to $\tilde{P}_V(t, l)$ as n grows.

We illustrate Theorem 3.1 by comparing between the discrete and continuous projections of the Shepp-Logan head phantom (Fig. 1). The Shepp-Logan head phantom is widely used in CT for testing the quality of reconstruction algorithms. The advantage of this phantom is that an analytic expression for its projections can be derived. Let $f(x, y)$ be the density function for the Shepp-Logan phantom. It is a sum of indicator functions of ellipses, weighted by the density of each ellipse. The function $f(x, y)$ equals zero outside the square $[-1, 1] \times [-1, 1]$. Notice that the Shepp-Logan phantom is not a Lipschitz function, which violates the conditions of Theorem 3.1. Nonetheless, discrete projections of the phantom closely approximate continuous ones, as we will see below.

We fix the resolution n and consider a discrete image $I(u, v) = f(u \frac{2}{n}, v \frac{2}{n})$, $u, v \in [-\frac{n}{2}, \frac{n}{2} - 1]$. We compute the 2D discrete Radon transform for this image, which results in two arrays of



Figure 1: Shepp-Logan head phantom

n	64	128	256	512	1024
Error	0.0782	0.0388	0.02	0.0097	0.0051

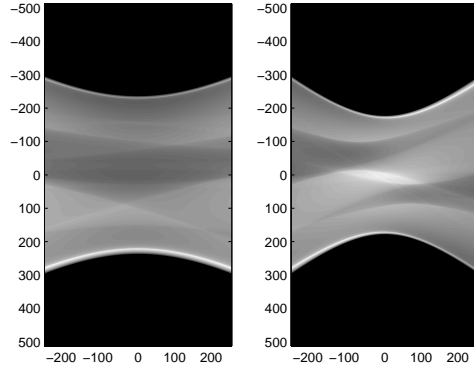
Table 1: Relative l_2 error between analytic and approximated projections

projections P_H and P_V . We multiply both arrays by $\frac{2}{n}$ to approximate continuous projections. The scaled arrays for the case $n = 512$ are displayed in Fig. 2(a).

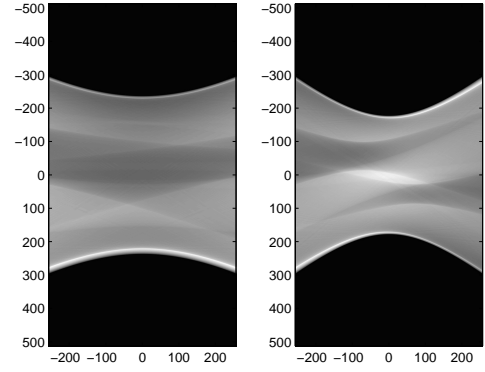
We then compute the two arrays \tilde{P}_H and \tilde{P}_V of the continuous projections of $f(x, y)$ (See Fig. 2(b) for illustration). It follows from Theorem 3.1 that the entries in P_H and P_V approximate the entries of \tilde{P}_H and \tilde{P}_V . In our example, the computed relative l_2 error between the arrays in Figs. 2(a) and 2(b) equals 0.0097. Table 1 gives relative l_2 errors between analytic and approximate projections of the Shepp-Logan phantom for different values of n .

We observe that in the case of the Shepp-Logan phantom the relative l_2 error decays like $\frac{5}{n}$, i.e. the error is inversely proportional to n .

Another way to estimate the quality of the approximations is to compute relative l_2 error separately for each projection. Figure 3 displays graphs of the error as a function of the

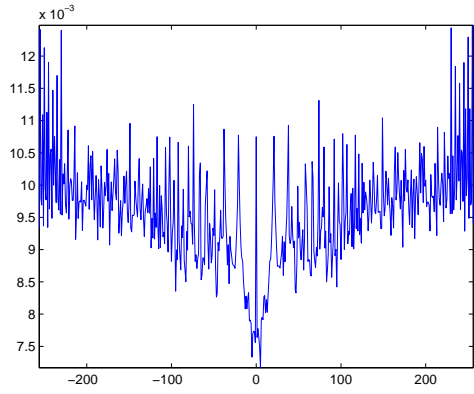


(a) P_H and P_V

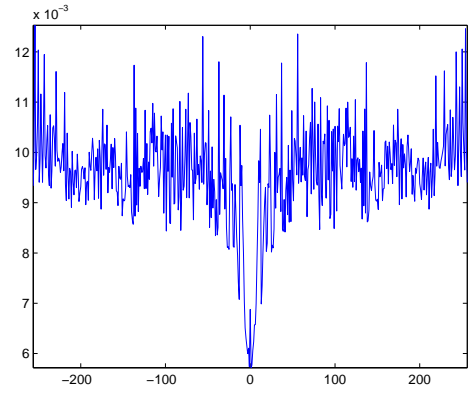


(b) \tilde{P}_H and \tilde{P}_V

Figure 2: Discrete projections vs. continuous projections



(a) Basically horizontal



(b) Basically vertical

Figure 3: Relative l_2 error as a function of projection number l

projection index $l \in [-n/2 : n/2]$ for $n = 512$.

Convergence of the discrete projections to continuous projections implies that we can reconstruct $f(x, y)$ from its continuous projections by applying the 2D inverse discrete Radon transform.

The discrete Radon transform [5] has both forward and inverse algorithms with complexity $O(n^2 \log n)$ for images of size $n \times n$. We briefly describe the inversion algorithms, as they are the main ingredient of the proposed reconstruction procedure. There are two inversion approaches, namely, an iterative one and a direct one. In both cases we use the discrete version of the Fourier slice theorem [5] to transform the problem from the Radon domain into the Fourier domain, thus formulating the reconstruction problem as the inversion of a non-uniform Fourier transform on a certain non-uniform grid. The resulting frequency grid is the so-called pseudo-polar grid [4].

The iterative algorithm is based on the application of the conjugate-gradient method to the Gram operator of the pseudo-polar Fourier transform. Since both the forward pseudo-polar Fourier transform and its adjoint can be computed in $O(n^2 \log n)$ operations, where $n \times n$ is the size of the input image, the Gram operator can also be computed in the same complexity. More specifically, both the pseudo-polar Fourier transform and its adjoint can be computed using $100n \log n$ operations (plus small lower order terms). This sums to $200n \log n$ operations per iteration. For comparison, the 2D FFT of a $n \times n$ image requires $25n \log n$ operations. The number of iterations is shown in [4] to be small for any practical image size (less than 6 iterations).

The advantage of the iterative inversion algorithm is its simplicity. On the other hand, it does not utilize the special frequency domain structure of the transform, and its execution time depends on the specific image to invert. Thus, [4] provides also a direct inversion algorithm, which directly resamples the pseudo-polar grid to a Cartesian frequency grid, and then, recovers the image from the Cartesian frequency grid. The algorithm is based on an “onion-peeling” procedure that at each step recovers two rows/columns of the Cartesian frequency grid, from

n	64	128	256	512
Error	0.33	0.22	0.16	0.11

Table 2: Reconstruction error for different n

the outermost rows/columns to the origin, by using columns/rows recovered in previous steps. The Cartesian samples of each row/column are recovered using trigonometric interpolation that is based on a Fast Multipole Method (FMM). Finally, the original image is recovered from the Cartesian frequency samples, which are not the standard DFT samples, by using a fast Toeplitz solver. For full details on both algorithms see [4].

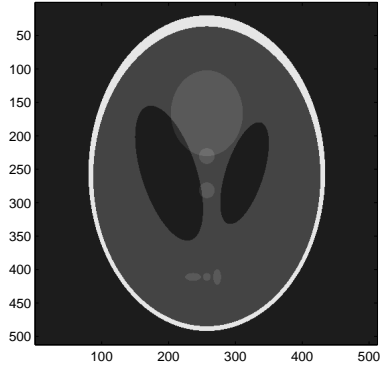
4 Reconstruction from parallel continuous projections

In this section we provide numerical evidence that the inverse discrete Radon transform produces high quality reconstructions from samples of the continuous Radon transform. The numerical examples are based on analytically computed parallel projections of the Shepp-Logan phantom.

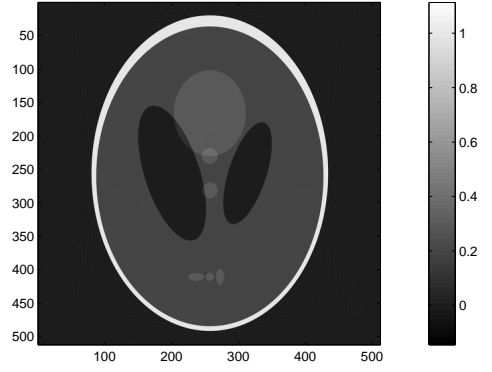
Let $f(x, y)$ denote the continuous Shepp-Logan phantom. For a fixed n , we compute the same line integrals of $f(x, y)$ as in Section 3, thus obtaining two arrays $\tilde{P}_H(t, l)$ and $\tilde{P}_V(t, l)$, $l \in [-\frac{n}{2}, \frac{n}{2}]$ and $t \in [-n, n]$. Then, we apply the 2D inverse discrete Radon transform to $\tilde{P}_H(t, l) \cdot \frac{n}{2}$ and $\tilde{P}_V(t, l) \cdot \frac{n}{2}$, obtaining a $n \times n$ image that approximates the original phantom sampled at points $\{(u\frac{2}{n}, v\frac{2}{n}) \mid u, v \in [-\frac{n}{2} : \frac{n}{2} - 1]\}$. The original and reconstructed phantoms, sampled with $n = 512$, are displayed in Figs. 4(a) and 4(b), respectively. The absolute value of the difference between these two images is shown in Fig. 5.

The reconstruction quality for $n = 64, 128, 256$ and 512 is illustrated by Fig. 6. The corresponding relative l_2 -errors are displayed in Table 2.

In Fig. 7(a) we provide a vertical profile of the original Shepp-Logan phantom (solid line) and its reconstruction for $n = 512$ (dotted line). A zoom on the central portion of the slice is



(a) Sampled Shepp-Logan



(b) Recovered Shepp-Logan

Figure 4: Sampled Shepp-Logan (left), recovery from projections by the inverse 2D Radon (right)

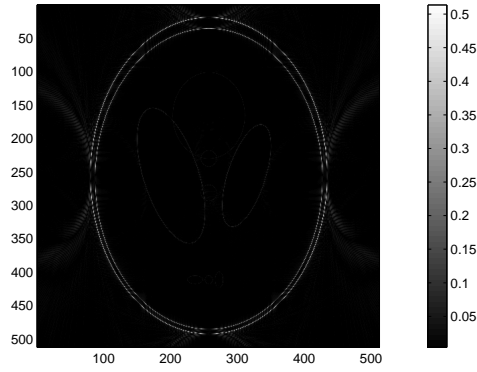
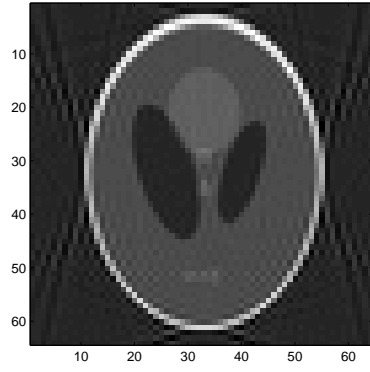
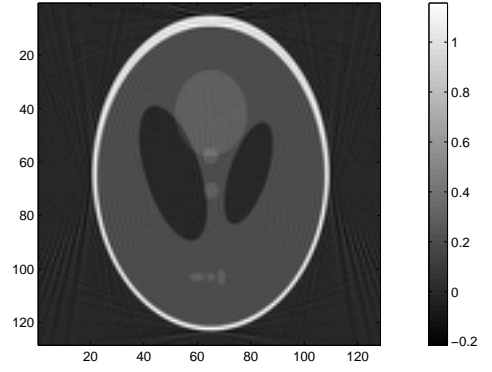


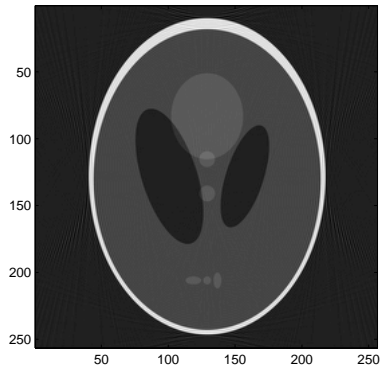
Figure 5: Reconstruction error



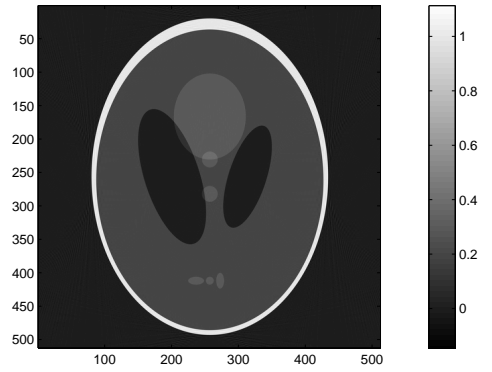
(a) $n = 64$



(b) $n = 128$

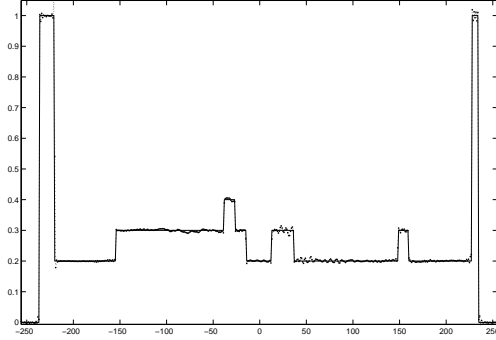


(c) $n = 256$

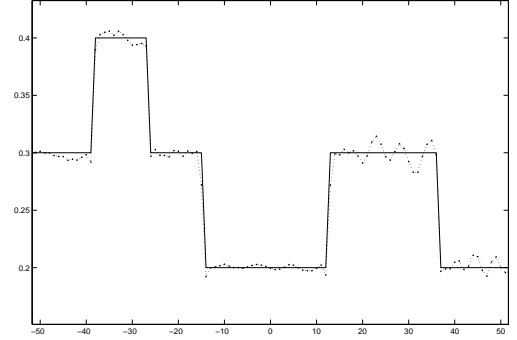


(d) $n = 512$

Figure 6: Reconstructed Shepp-Logan for $n = 64, 128, 256, 512$



(a) Vertical profile



(b) Zoom of the central portion

Figure 7: Vertical profile of the phantom (solid line), and its reconstruction (dotted line)

shown on Fig. 7(b).

5 Fan-beam reconstruction

In Section 4 we showed that the 2D inverse discrete Radon transform can be used for the reconstruction of an object from its continuous projections along lines from \tilde{S}_H and \tilde{S}_V .

Collecting this set of projections by a single pair of source/detector is a time-consuming operation, since for each projection angle the source/detector pair should scan linearly over the orthogonal direction, collecting $2(n+1)$ line integrals. This process should be repeated for each projection angle. Overall, the point source should be turned on and off $2(n+1)(2n+1)$ times in order to collect the required projections.

In this section we show that if we can afford using multiple detectors with a single radiation source (as is the case with contemporary scanners), we can efficiently collect all the required line projections using certain fan-beam projections. The process that composes parallel projections from lines that were collected using fan-beam projections is usually referred to as “re-sorting”.

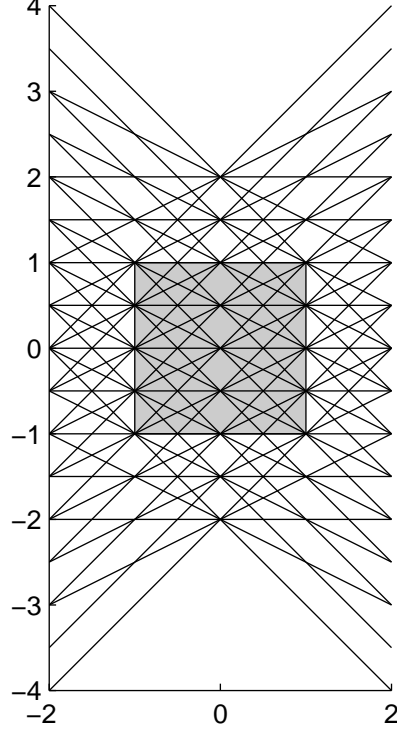


Figure 8: Basically horizontal lines for $n = 4$

5.1 Acquisition geometry

We consider a 2D object, described by $f(x, y)$, such that $f(x, y) = 0$ outside $[-1, 1] \times [-1, 1]$. For $n = 4$, we draw all the lines from \tilde{S}_H in Fig. 8. All the line integrals in this figure can be collected using fan-beam projections with sources on the line $x = -2$. This is true for any n . Indeed, y -coordinates of points of intersection of lines from \tilde{S}_H with the vertical line $x = -2$ are $y = -\frac{4l}{n} + \frac{2}{n}t$, which are multiples of $\frac{2}{n}$ by an integer from $[-2n : 2n]$.

Points of intersection between basically horizontal lines and the vertical line $x = 2$ are $y = -\frac{4l}{n} + \frac{2}{n}t$, which are also multiples of $\frac{2}{n}$ by an integer from $[-2n : 2n]$. Therefore, each line

from \tilde{S}_H can be uniquely defined as the line that passes through the two points $(-2, \frac{2}{n}z)$ and $(2, \frac{2}{n}w)$, $z, w \in [-2n : 2n]$.

By placing the set of detectors at the points $(2, \frac{2}{n}w)$, $w \in [-2n : 2n]$, and successively placing the radiation source at points $(-2, \frac{2}{n}z)$, $z \in [-2n : 2n]$, we can collect all the projections from \tilde{S}_H . By swapping axes we can collect in the same way the projections along lines from \tilde{S}_V . Therefore, all the line projections required in order to reconstruct a $n \times n$ discrete approximation of $f(x, y)$ using 2D inverse discrete Radon transform are contained in $(4n+1) + (4n+1) = 8n+2$ fan-beam projections, where the radiation source moves along a straight line with equal steps.

As we mentioned above, each line in \tilde{S}_H can be described either by the parameters (l, t) , $l \in [-\frac{n}{2} : \frac{n}{2}]$ and $t \in [-n, n]$, or by the pair (z, w) , $z, w \in [-2n : 2n]$. In Section 5.2 we establish the correspondence between these two representations.

5.2 Re-sorting algorithm

Consider a point $(-2, \frac{2}{n}z)$, $z \in [-2n : 2n]$. We want to find which lines from \tilde{S}_H pass through this point. Formally, for each $z \in [-2n : 2n]$ we want to find the set

$$S_z = \{(l, t) \mid \frac{2}{n}z = \frac{2l}{n}(-2) + \frac{2}{n}t, \quad l \in [-\frac{n}{2} : \frac{n}{2}], \quad t \in [-n : n]\}.$$

We get

$$S_z = \{(l, t) \mid z = -2l + t, \quad l \in [-\frac{n}{2} : \frac{n}{2}], \quad t \in [-n : n]\}.$$

If we consider a plane with Cartesian coordinates l and z , then $z = -2l + t$ is a straight line equation with slope -2 that intersects the z -axis at t . For $l \in [-\frac{n}{2}, \frac{n}{2}]$ and $t \in [-n, n]$, the points (l, z) cover a parallelogram with vertices at $(-\frac{n}{2}, 2n), (-\frac{n}{2}, 0), (\frac{n}{2}, 0)$ and $(\frac{n}{2}, -2n)$.

Therefore, for each $z \in [0, 2n]$ there exists $t \in [-n, n]$ such that $z = -2l + t$ if and only if $l \in [-\frac{n}{2}, \frac{n-z}{2}]$. Similarly, for each $z \in [-2n, 0]$ there exists $t \in [-n, n]$ such that $z = -2l + t$ if and only if $l \in [-\frac{n+z}{2}, \frac{n}{2}]$.

We now return to the task of finding S_z . We consider four cases, depending on whether z is even or odd and whether z is positive or negative.

Theorem 5.1. For $z \in [-2n : 2n]$, the set S_z is given by the following formulae:

Case $z = 2k$, $k \in [0 : n]$

$$S_z = \{(l, z + 2l) \mid l \in [-\frac{n}{2} : \frac{n-z}{2}]\}.$$

Case $z = 2k - 1$, $k \in [1 : n]$

$$S_z = \{(l, z + 2l) \mid l \in [-\frac{n}{2} : \frac{n-z-1}{2}]\}.$$

Case $z = -2k$, $k \in [1 : n]$

$$S_z = \{(l, z + 2l) \mid l \in [\frac{-n-z}{2} : \frac{n}{2}]\}.$$

Case $z = -2k + 1$, $k \in [1 : n]$

$$S_z = \{(l, z + 2l) \mid l \in [\frac{-n-z+1}{2} : \frac{n}{2}]\}.$$

Proof. We prove the case $z = 2k - 1$, $k \in [1 : n]$. It follows from the geometric considerations above that there exists $t \in [-n, n]$ such that $z = -2l + t$ if and only if $l \in [-\frac{n}{2}, \frac{n-z}{2}]$, that is $l \in [-\frac{n}{2}, \frac{n}{2} - k + \frac{1}{2}]$. Since we are looking for an integer l , this is equivalent to $l \in [-\frac{n}{2} : \frac{n}{2} - k]$ which is, in turn, equivalent to $l \in [-\frac{n}{2} : \frac{n-z-1}{2}]$.

Since $z = -2l + t$, we have $t = z + 2l$. Consequently $S_z = \{(l, z + 2l) \mid l \in [-\frac{n}{2} : \frac{n-z-1}{2}]\}$.

The proofs of the other cases are similar. \square

Corollary 5.2. The pair (z, w) defines a line from \tilde{S}_H if and only if $z, w \in [-2n : 2n]$ and $w = z + 4l$ for some $l \in S_L(z)$, where $S_L(z)$ is defined as follows:

Case $z = 2k$, $k \in [0 : n]$

$$S_L(z) = [-\frac{n}{2} : \frac{n-z}{2}].$$

Case $z = 2k - 1$, $k \in [1 : n]$

$$S_L(z) = [-\frac{n}{2} : \frac{n-z-1}{2}].$$

Case $z = -2k$, $k \in [1 : n]$

$$S_L(z) = [\frac{-n-z}{2} : \frac{n}{2}].$$

Case $z = -2k + 1$, $k \in [1 : n]$

$$S_L(z) = [\frac{-n-z+1}{2} : \frac{n}{2}].$$

Proof. It follows immediately from Theorem 5.1 and the fact that (z, w) defines some line from \tilde{S}_H if and only if there exist $l \in [-\frac{n}{2}, \frac{n}{2}]$ and $t \in [-n, n]$ such that $z = -2l + t$ and $w = 2l + t$. \square

For each pair (l, t) that defines a line from \tilde{S}_H we can find $(\frac{2}{n}z, \frac{2}{n}w)$ as the points of intersection of this line with the vertical lines $x = -2$ and $x = 2$. Therefore,

$$z = \frac{2l}{n}(-n) + t = -2l + t$$

$$w = \frac{2l}{n}(n) + t = 2l + t.$$

Vice versa, if the pair (z, w) defines a line from \tilde{S}_H (which we can check using Corollary 5.2), then the parameters (l, t) are

$$t = \frac{w+z}{2} \quad l = \frac{w-z}{4}.$$

We now describe the algorithm for collecting the set of line projections $\tilde{P}_H(t, l)$ using fan-beam projections. As usual, we assume that the object under consideration fits within the box $[-1, 1] \times [-1, 1]$. Detectors are placed at the points $(2, \frac{2}{n}w)$, $w \in [-2n : 2n]$. Each fan-beam projection is acquired by placing the radiation source at one of the points $(-2, \frac{2}{n}z)$, where $z \in [-2n : 2n]$. We denote by $P_z(w)$ the output of the detector located at $(2, \frac{2}{n}w)$ when the object is illuminated by the point source located at $(-2, \frac{2}{n}z)$. For a fixed $z \in [-2n : 2n]$, we set $\tilde{P}_H(\frac{w-z}{4}, \frac{w+z}{2}) = P_z(w)$ for all $w \in \{z + 4l \mid l \in S_z(l)\}$. The algorithm that collects \tilde{P}_V is identical up to a swap of the axes.

It is important to notice here, that we have a choice of either collecting data for all pairs (z, w) and then selecting the pairs that correspond to lines from \tilde{S}_H , or collecting only necessary

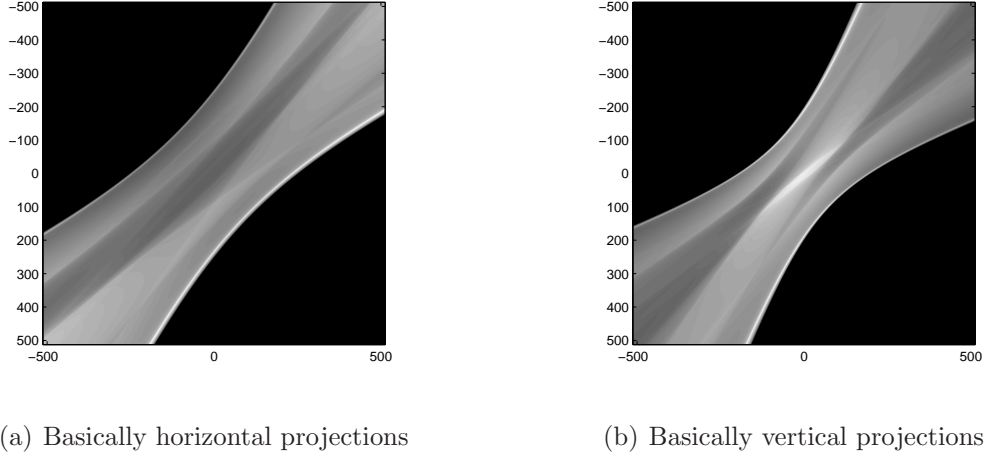


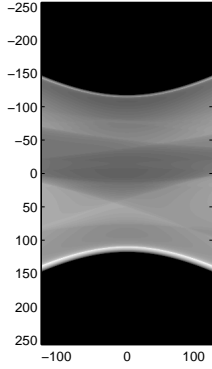
Figure 9: Fan-beam projections for $n = 256$

projections from the beginning, discarding the output of detectors for which the line given by (z, w) is not within \tilde{S}_H .

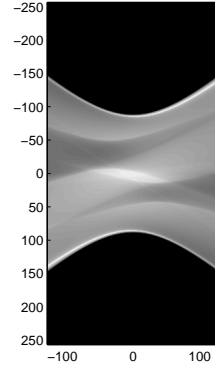
5.3 Numerical results

We next give an example of reconstructing the Shepp-Logan phantom from fan-beam projections. First, we compute the full set of analytic fan-beam projections of the Shepp-Logan phantom for $n = 256$. Figure 5.3 displays two $(4n + 1) \times (4n + 1)$ arrays $\tilde{F}_H(z, w)$ and $\tilde{F}_V(z, w)$, which are formed by fan-beam projections in (z, w) -coordinates. The z -th row of the left array is the fan-beam projection with source placed at $(-2, \frac{2}{n}z)$ and detectors placed at $(2, \frac{2}{n}w)$, $w \in [-2n : 2n]$. The z -th row of the right array is the fan-beam projection with source placed at $(\frac{2}{n}z, -2)$ and detectors placed at $(\frac{2}{n}w, 2)$, $w \in [-2n : 2n]$.

From this set of fan-beam projections we construct the corresponding arrays of parallel projections, by applying the re-sorting algorithm of Section 5.2. Namely, for $l \in [-\frac{n}{2} : \frac{n}{2}]$ and $t \in [-n : n]$ we set $\tilde{P}_H(t, l) = \tilde{F}_H(\frac{w+z}{2}, \frac{w-z}{4})$ and $\tilde{P}_V(t, l) = \tilde{F}_V(\frac{w+z}{2}, \frac{w-z}{4})$. The resulting arrays are displayed in Fig. 5.3.



(a) Basically horizontal projections



(b) Basically vertical projections

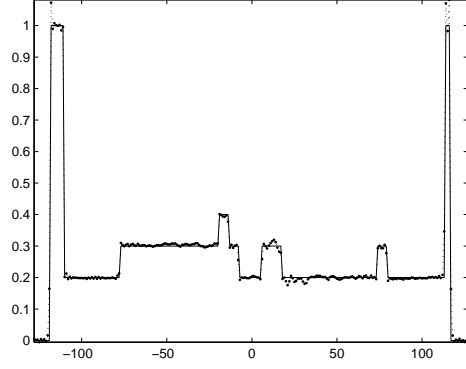
Figure 10: Re-sorted projections

Then, we apply the 2D inverse discrete Radon transform to obtain the discrete approximation of the Shepp-Logan phantom. The resulting reconstruction is exactly the same as we get from parallel projection using the approach described in section 4. The reconstructed image for the case $n = 256$ is displayed in Fig. 6(c).

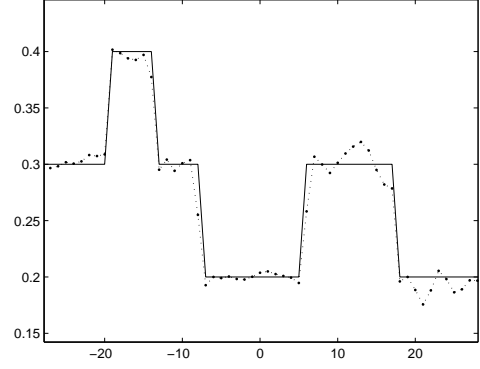
We provide a vertical profile (slice along the line $x = 0$) of the original Shepp-Logan phantom (solid line) and its reconstruction for $n = 256$ (dotted line) on Fig. 11(a). Zoom of the central portion of the slice is displayed on Fig. 11(b). Figures 12(a) and 12(b) show the horizontal profile (slice along the line $y = 0$) of the Shepp-Logan phantom and its reconstruction.

References

- [1] S. R. Deans, The Radon Transform and Some of Its Applications, New York: Wiley, 1983.
- [2] F. Natterer, The Mathematics of Computerized Tomography. New York: Wiley, 1986.

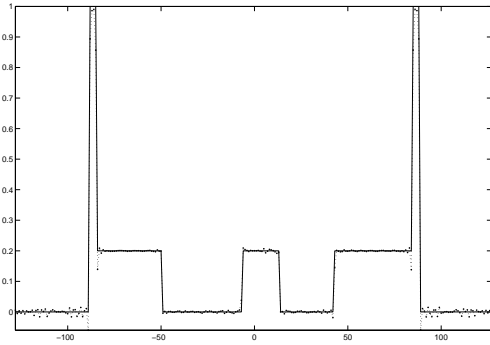


(a) Vertical profile

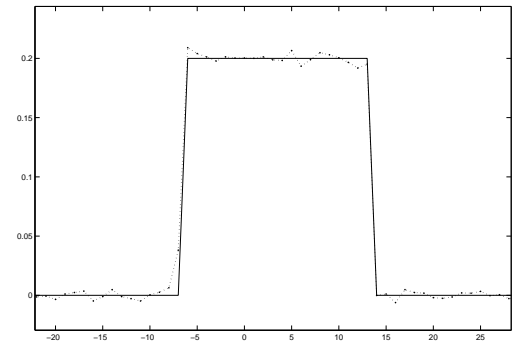


(b) Zoom of the central portion

Figure 11: Vertical profile of the phantom (solid line), and its reconstruction (dotted line) for $n = 256$



(a) Horizontal profile



(b) Zoom of the central portion

Figure 12: Horizontal profile of the phantom (solid line), and its reconstruction (dotted line) for $n = 256$

- [3] A. Kak and M. Slaney, Principles of Computerized Tomographic Imaging, New York: IEEE Press, 1988.
- [4] A. Averbuch, R.R. Coifman, D.L. Donoho, M. Israeli, Y. Shkolnisky, A framework for discrete integral transformations I – the pseudo-polar Fourier transform, submitted.
- [5] A. Averbuch, R.R. Coifman, D.L. Donoho, M. Israeli, Y. Shkolnisky and I. Sedelnikov, A framework for discrete integral transformations II – the 2D discrete Radon transform, submitted.
- [6] A. Brandt, J. Mann, M. Brodski, and M. Galun, A fast and accurate multilevel inversion of the radon transform, SIAM J. Appl. Math., 60(2), 437–462, 2000.
- [7] S. Basu, Y. Bresler, $O(N^2 \log_2 N)$ filtered backprojection reconstruction algorithm for tomography, IEEE Trans. on Image Processing, 9(10), pp. 1760–1773, 2000.
- [8] S. Basu, Y. Bresler, Error analysis and performance optimization of fast hierarchical back-projection algorithms, IEEE Trans. on Image Processing, 10(7), pp. 1103–1117, 2001.
- [9] S. Basu, Y. Bresler, Fast hierarchical backprojection method for imaging, USA Patent 6,282,257, 2001.
- [10] H. Schomberg and J. Timmer, The gridding method for image reconstruction by Fourier transformation, IEEE Trans. Med. Imag., 14(3), 596–607, 1995.